Purdue University
Purdue e-Pubs

Birck and NCN Publications | Birck Nanotechnology Center

4-13-2012

# A Physics-Based Predictive Modeling Framework for Dielectric Charging and Creep in RF MEMS Capacitive Switches and Varactors

Ankit Jain
jankit@purdue.edu

Sambit palit
*Purdue University*, spalit@purdue.edu

Muhammad Ashraful Alam
*Purdue University*

Follow this and additional works at: https://docs.lib.purdue.edu/nanopub

Part of the Electro-Mechanical Systems Commons, and the Electronic Devices and Semiconductor Manufacturing Commons

Jain, Ankit; palit, Sambit; and Alam, Muhammad Ashraful, "A Physics-Based Predictive Modeling Framework for Dielectric Charging and Creep in RF MEMS Capacitive Switches and Varactors" (2012). *Birck and NCN Publications.* Paper 861.
http://dx.doi.org/10.1109/JMEMS.2011.2174418

This document has been made available through Purdue e-Pubs, a service of the Purdue University Libraries. Please contact epubs@purdue.edu for additional information.

# A Physics-Based Predictive Modeling Framework for Dielectric Charging and Creep in RF MEMS Capacitive Switches and Varactors

Ankit Jain, Sambit Palit, *Student Member, IEEE*, and Muhammad Ashraful Alam, *Fellow, IEEE*

***Abstract*—In this paper, we develop a physics-based theoretical modeling framework to predict the device lifetime defined by the dominant degradation mechanisms of RF microelectromechanical systems (MEMS) capacitive switches (i.e., dielectric charging) and varactors (i.e., creep), respectively. Our model predicts the parametric degradation of performance metrics of RF MEMS capacitive switches and varactors, such as pull-in/pull-out voltages, pull-in time, impact velocity, and capacitance both for dc and ac bias. Specifically, for dielectric charging, the framework couples an experimentally validated theoretical model of time-dependent charge injection into the bulk traps with the Euler-Bernoulli equation for beam mechanics to predict the effect of dynamic charge injection on the performance of a capacitive switch. For creep, we generalize the Euler-Bernoulli equation to include a spring-dashpot model of viscoelasticity to predict the time-dependent capacitance change of a varactor due to creep. The new model will contribute to the reliability aware design and optimization of the capacitive MEMS switches and varactors. [2011-0086]**

***Index Terms*—Capacitance, creep, electrostatic actuators, microelectromechanical systems, reliability, switches, varactors.**

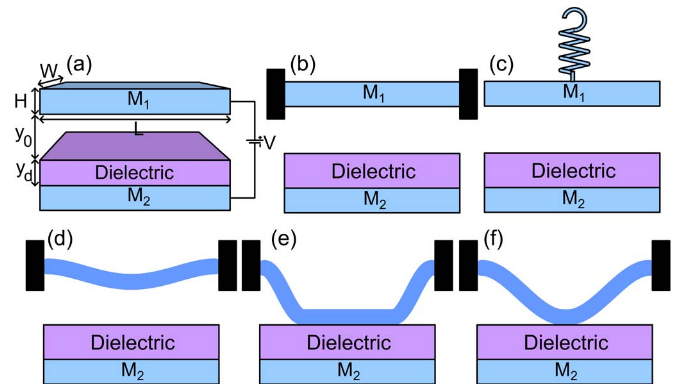


Fig. 1. (a) Schematic of RF MEMS capacitive switch/varactor, defining its physical parameters. (b) Schematic of the same with electrode $M_1$ modeled as a fixed-fixed beam. (c) Equivalent, 1-D spring-mass model. (d)–(f) Shapes of the deflected beam at different operating voltages: (d) before pull in, (e) after pull-in, (f) just before pull-out.

## I. Introduction

Radio frequency microelectromechanical systems (RF MEMS) are used in radar systems, wireless communication systems, and instrumentation [1] as ohmic and capacitive switches, tunable capacitors or varactors, high $Q$ inductors, transmission lines, microwave, and millimeter wave elements [2]. Specifically, the *capacitive switches* are used for signal routing, impedance matching networks, and adjustable gain amplifiers. These switches have lower-power consumption, lower insertion and return loss, higher RF linearity and better isolation compared to their semiconductor counterparts like Si Field Effect Transistors (FETs), GaAs Metal Semiconductors FETs, and p-i-n (PIN) diodes [2]–[4]. Here, RF linearity is defined by the degree to which the output RF signal is distorted with respect to the input signal when a MEMS switch is inserted in the channel (and should not be confused with the nonlinear actuation of the MEMS switch itself). Likewise, *varactors* find applications in low noise parametric amplifiers, harmonic frequency generators, and voltage controlled oscillators. In these cases, classical varactors based on Si or GaAs p-n or Schottky junction diodes do not provide adequate tuning, sufficient RF linearity, high enough quality factor, and higher self-resonance frequency as compared to RF MEMS varactors. As a generic platform, the RF MEMS capacitive switches and varactors have similar physical structure [Fig. 1(a)–(c)], with two metal surfaces (electrodes) separated by a sandwich of an air gap and a thin dielectric (absent in some varactors). In both cases, upper electrode $M_1$ moves toward the fixed electrode $M_2$ in response to the applied voltage $V$. The only difference is that varactors operate in an analog mode, with the gap changing continuously as a function of $V$ (below the pull-in state), whereas switches operate in the binary mode between "up" (below pull-in) and "down" (above pull-in) states.

Despite many advantages of RF MEMS, their large-scale deployment has been stymied by several reliability issues such as stiction [4], [5], mechanical fatigue [6], creep [7], contact degradation [8], and dielectric charging [9]. To be commercially viable, these switches must satisfy stringent reliability requirements of failure-free operation over billions of cycles. Despite this importance, however, relatively few modeling efforts have discussed the issues of electromechanical reliability within a comprehensive theoretical framework. *Developing such a framework is the key goal of this paper.*

Manuscript received March 21, 2011; revised September 6, 2011; accepted September 26, 2011. Date of publication December 8, 2011; date of current version April 4, 2012. This work was supported by the MIT-MSD and PRISM centers. Subject Editor N. Aluru.

The authors are with the School of Electrical and Computer Engineering, Purdue University, West Lafayette, IN 47907-2035 USA (e-mail: jankit@purdue.edu; spalit@purdue.edu; alam@purdue.edu).

Color versions of one or more of the figures in this paper are available online at http://ieeexplore.ieee.org.

Digital Object Identifier 10.1109/JMEMS.2011.2174418

1057-7157/$26.00 © 2011 IEEE

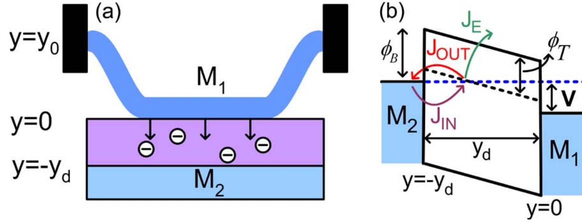


Fig. 2. (a) Schematic of the MEMS switch showing charge injection into the bulk traps inside the dielectric when fixed-fixed beam is pulled-in. (b) The band diagram of a metal-insulator-metal system defining the barrier heights and current components into and out of the traps. Voltage $V$ has been applied between the electrode $M_1$ and $M_2$.

Among the several reliability issues of RF MEMS capacitive switches, dielectric charging [10], [11] is arguably the most important. When the movable electrode $M_1$ is pulled-in [down state, Fig. 2(a)], charges are injected into the traps/defects inside the dielectric. These trapped charges modify the electrostatic force acting on $M_1$, and cause the capacitance versus voltage (CV) curve to shift, and the $Vp_I/Vp_O$ to change over time. This parametric degradation eventually leads to catastrophic failure by stiction: the electrode $M_1$ can no longer be restored to its pulled-up state even at zero voltage (i.e., $Vp_O < 0$), because the downward electrostatic force exerted by the accumulated charges within the dielectric now exceeds the restoring spring force. We will, therefore, define the lifetime ($t_{\rm life}$) of the device due to dielectric charging by the condition $Vp_O(t_{\rm life}) = 0$. To predict $t_{\rm life}$, three key factors should be considered: 1) physical mechanism of time-dependent charge injection into the dielectric, 2) modification of electrostatic force due to injected charges, and 3) evolution of $Vp_O$ as a function of time. In the literature, time dynamics of $Vp_O$ is modeled either by a simple first-order resistor-capacitor model, with its time constants fitted to experimental data [12]–[14], or by considering the injected charge simply as an input parameter [15], [16]. Therefore, it is difficult to know if the predictions from these empirical models are reliable, or how sensitive the model is to the changes in physical parameters such as trap density and barrier height, arising from changes in the fabrication conditions.

Similarly, the dependence of $t_{\rm life}$ on the stress voltage $V$ has been studied experimentally, and a basic model $t_{\rm life} \sim \exp(-\gamma V)$ has been observed to fit the data [12], [17], [18], where $\gamma$ is the voltage acceleration factor. This "exponential" model has been derived by assuming Frenkel-Poole (FP) charge injection [10], [18], but the applicability of FP conduction to the dielectrics used in RF MEMS (∼100–500 nm) is questionable [19]. Generally speaking, therefore, the field lacks a physics-based theoretical model/framework which can anticipate time evolution of $Vp_I/Vp_O$ and predict $t_{\rm life}$ as a function of voltage and duty cycle. In this article, we first develop a model for time-dependent charge injection inside the dielectric and couple it with the Euler-Bernoulli (EB) equation (Section II). This is the *first key contribution* of the paper.

Varactors, on the other hand, operate below $Vp_I$ and are therefore safe from stiction. It has been observed, however, that a sustained dc bias causes electrode $M_1$ to continuously sag from its steady-state equilibrium position, resulting in the steady increase in the capacitance [20], [21]. The change in the capacitance degrades the tuning range of the varactor. This phenomenon has been attributed to creep [20], [21], and has been studied using viscoelastic theory [20], [22]. In the literature, experimentally derived dynamic spring constant was used to study the resonator's frequency degradation over time [20]. When generalized to a CAD model, it allows us to explore "creep compliance" as a function of time and interpret the characteristics of resonators and phase shifters [23]. Unfortunately, this *empirical lumped-parameter spring-mass model* [Fig. 1(c)] can neither account for the position-resolved bending of the upper electrode as a function of time, nor does it address the "creep-limited lifetime" of the varactors. We define "creep-limited lifetime" as the time needed to cross a certain predefined (and circuit-specific) threshold of capacitance degradation due to creep. In this article, we generalize the EB equation to include a spring-dashpot model of viscoelasticity to predict the shape of the upper electrode as a function of time and voltage. This model allows us to predict parametric degradation of varactor performance and the associated creep-limited lifetime. This is the *second key contribution* of the paper.

The paper has the following seven objectives: 1) couple the time-dependent charge injection with the EB equation to establish a scaling relationship for time dynamics of pull-out voltage, i.e., $\Delta Vp_O(t) = g(t/t_{\rm life}) \sim (t/t_{\rm life}(V))^\beta$, where $\beta$ is device-specific constant, 2) show that the number of cycles of reliable operation of a capacitive switch is given by $N_{\rm life} = t_{\rm life}(V)/(d_c T - tp_I(V))$, where $d_c$ is the duty cycle, $tp_I$ is the pull-in time, and $f = 1/T$ is the frequency of operation of actuation voltage, 3) demonstrate that the lifetime predicted by the empirical "exponential model" is unduly pessimistic; physics of charge injection within the dielectric anticipates a more optimistic superexponential voltage scaling, (i.e., $t_{\rm life} \gg \exp(-\gamma V)$, 4) show that the dynamic charge injection within the dielectric increases the impact velocity $v_{\rm impact}$, which may further degrade surface morphology of the dielectric, 5) generalize the EB equation to include a spring-dashpot model of viscoelasticity to predict the effect of creep on the time-dependent capacitance change under dc/ac bias, 6) predict the creep-limited $t_{\rm life}$ of a varactor, and finally, 7) study the effect of duty cycle on creep-induced capacitance change.

The rest of the paper is organized as follows. In Section II, we describe models for static and dynamic behavior of RF MEMS switches/varactors using the EB equation, with the explicit goals of obtaining, $C(V)$, $Vp_I$, $Vp_O$, $tp_I(V)$, and $v_{\rm impact}(V)$ needed for dielectric charging and creep reliability models. We then discuss the techniques to include dielectric charging and creep degradation mechanisms within the EB framework. In Section III, we first validate the model with the experimental data, and then use the model to explore the new, nonintuitive predictions discussed above. Section IV summarizes the findings of this paper and highlights the limitations of our approach, suggesting opportunities for further contributions.

## II. Model Description

### A. *Euler-Bernoulli Equation for the Beam Shape*

Since the essential aspects of the dynamics of RF MEMS switches/varactors under electrostatic actuation have been

discussed extensively by many groups [24]–[30], here we only sketch the key elements of the problem for completeness. Fig. 1(a) shows the schematic of a RF MEMS capacitive switch/varactor, which involves a movable metal electrode $M_1$, air gap, a dielectric, and a fixed electrode $M_2$. This movable electrode $M_1$ is modeled as a fixed-fixed beam [Fig. 1(b)]. When a voltage is applied between electrode $M_1$ and $M_2$, fixed-fixed beam bends down symmetrically. Fig. 1(d)–(f) shows the shape of the beam before pull-in [Fig. 1(d)], after pull-in [Fig. 1(e)], and just before pull-out [Fig. 1(f)]. The shapes of the beam can be calculated by solving the widely used EB equation for the beam dynamics [26], [30], i.e.,

$$\rho W H \frac{\partial^2 y(x,t)}{\partial t^2} + b(y)\frac{\partial y(x,t)}{\partial t} + \frac{EI}{1-v^2}\frac{\partial^4 y(x,t)}{\partial x^4} = F_{\text{electrostatic}} = \frac{W\epsilon_0\epsilon_r^2 V^2}{2\left(y_d+\epsilon_r y(x,t)\right)2} \quad (1)$$

where $\rho$ is the density of the beam, $W$ is the width of the beam, $H$ is the thickness of the beam, $y$ is the deflection at location $x$, and $x$ is along the length of the beam. $t$ is the time, $b(y)$ is the squeeze film gas damping coefficient [31]–[33], $E$ is the young's modulus of the beam, $I(=(WH^3/12))$ is the second moment of area of the beam, and $v$ is the Poisson's ratio of the beam. Right-hand side of (1) is the electrostatic force per unit length acting on the electrode $M_1$, where, $\epsilon_0$ is the permittivity of free space, $\epsilon_r$ is the dielectric constant of the dielectric, $V$ is the applied voltage, and $y_d$ is the dielectric thickness. In the specific example of fixed-fixed beam, two ends of the beam are fixed at $y = y_0$, and the slope $\partial y/\partial x$ vanishes at its two ends. This is mathematically represented by the following boundary conditions:

$$y(0,t) = y(L,t) = y_0 \quad (2a)$$

$$\frac{\partial y}{\partial x}(0,t) = \frac{\partial y}{\partial x}(L,t) = 0 \quad (2b)$$

where $L$ is the length of the beam, and $y_0$ is the air gap. Since our focus is on calculating the reliability-limited lifetimes of RF MEMS capacitive switches/varactors, we do not include further details of the beam dynamics typical of more comprehensive models, such as the deflection of the electrode $M_1$ along the width direction (full 3-D model) [27], fringing fields [28], midplane stretching [34], and the residual stress [29] in the as-fabricated device. These additional features are not expected to change the qualitative features of our predictions and are reserved for future work on this topic.

### B. Degradation Mechanisms

In this section, we discuss the theoretical models of dielectric charging and creep, and techniques to combine them with the EB equation (1) for the prediction of $t_{\text{life}}$ due to these degradations.

*1) Dielectric Charging:* There is a long history of modeling and experiments related to charge injection into the dielectric, details of which can be found in references [35]–[38]. Here, we only highlight the relevant features/equations of dielectric charging related to RF MEMS capacitive switches. During the pulled-in state, the switch can be modeled as a metal-insulator-metal (MIM) system. Fig. 2(b) shows the band diagram of the MIM system, showing the location of a trap in energy, barrier height $\Phi_B$, and three trapping/detrapping ($J_{IN}$, $J_{OUT}$, and $J_E$) fluxes into and out of the traps. The traps are assumed electrically neutral (before charge injection from the contact), uniformly distributed within the dielectric with density $N_T$, with a tunneling capture cross section $\sigma$, and located at an energy level $\Phi_T$ below the dielectric conduction band [39]. The three trapping/detrapping fluxes are based on the following processes: 1) electrons injected from the metal contacts into traps by tunneling ($J_{IN}$), 2) electrons tunneling out from the traps back into the contact ($J_{OUT}$), and/or 3) electrons emitted out of the traps into the dielectric conduction band by a field-assisted, temperature-activated FP emission process ($J_E$). The expressions for $J_{IN}(y)$, $J_{OUT}(y)$, and $J_E(y)$ in terms of trapped electron density $n_T(y,t)$ and device-specific constants $A_{IN}(y)$, $A_{OUT}(y)$, and $A_E(y)$, (details of which can be found in the section I of the Appendix) are given by (3).

$$J_{IN}(y) = A_{IN}(y)\left[N_T - n_T(y,t)\right] \quad (3a)$$

$$J_{OUT}(y) = A_{OUT}(y) n_T(y,t) \quad (3b)$$

$$J_E(y) = A_E(y) n_T(y,t). \quad (3c)$$

The rate of change of $n_T(y,t)$ is given by the balance of current fluxes going into and coming out of the traps, i.e.,

$$q\Delta y \frac{dn_T(y,t)}{dt} = J_{IN}(y) - J_{OUT}(y) - J_E(y). \quad (4)$$

The solution of (4) provides the time dynamics of $n_T(y,t)$. These trapped charges modify the electrostatic force (5) acting on the electrode $M_1$ as follows:

$$F_{\text{electrostatic}} = \frac{W\epsilon_0\epsilon_r^2\left(V-\Delta V(t)\right)^2}{2(y_d+\epsilon_r y)^2},$$

$$\Delta V(t) = -\frac{q}{\epsilon_0\epsilon_r}\int_{-y_d}^{0} y n_T(y,t)dy. \quad (5)$$

Equations (1) and (2) can now be solved with the modified electrostatic force (5) to study the effect of dielectric charging on $Vp_I/Vp_O$, $tp_I$, $v_{\text{impact}}$, and $t_{\text{life}}$.

*2) Creep:* Creep is a time-dependent deformation phenomenon during which a material deforms when subjected to a constant load (or stress) for a prolonged period of time [40]. The creep in RF MEMS varactors has been studied using theory of viscoelasticity [20], [22]. A viscoelastic material can be represented as a combination of linear spring (elastic element) and a dashpot (viscous element) (Fig. 3) [41]. The linear spring follows the Hooke's law, $\sigma = E\epsilon$, where, $\sigma$ is the stress, $\epsilon$ is the strain, and $E$ is the Young's modulus, whereas the dashpot follows the Newton's law $\sigma = \eta(d\epsilon/dt)$, where, $\eta$ is the viscosity of material. The elastic and viscous components experience the same strain when they are in parallel, but the total strain is the sum of the two strains when they are in series. A model of creep with multiple time constants, as

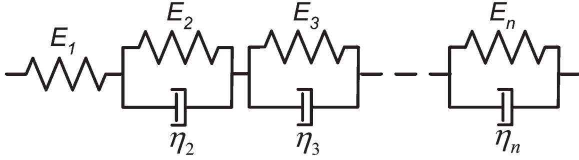


Fig. 3. Spring-dashpot model of a viscoelastic material. The spring is a linear element and follows $\sigma = E\epsilon$, whereas the dashpot follows $\sigma = \eta(d\epsilon/dt)$. We use this model to generalize the EB equation (7) to account for the creep behavior observed in RF MEMS varactors.

shown in Fig. 3, can be defined by the following stress-strain relationship:

$$\frac{\sigma}{E_i} = \frac{\eta_i}{E_i}\frac{d\epsilon_i}{dt} + \epsilon_i, \quad i = 2, \ldots, n \tag{6a}$$

$$\epsilon = \frac{\sigma}{E_1} + \sum_2^n \epsilon_i \tag{6b}$$

where $E_i$, is the Young's modulus, $\eta_i$ is the viscosity, $\epsilon_i$ is the strain of the $i$th branch of the model, $\sigma$ is the total stress, and $\epsilon$ is the total strain.

The steady-state EB equation [(1), with time derivative set to zero] describes the steady-state elastic response $(\sigma = E\epsilon)$ of the beam. It is, however, necessary to use a time-dependent stress-strain relationship (6) for modeling the creep behavior of the varactors. The following generalized EB equation [(7), derived in section II of the Appendix], accounts for the "spring-dashpot" response of the beam, and allows us to interpret the time-dependent creep phenomena observed experimentally.

$$E_1 I \frac{\partial^4 y}{\partial x^4} = F_{\text{electrostatic}} + E_1 I \sum_2^n \epsilon_i^m \tag{7a}$$

$$\frac{F_{\text{electrostatic}}}{E_i I} = \frac{\eta_i}{E_i}\frac{d\epsilon_i^m}{dt} + \epsilon_i^m, \quad i = 2, \ldots n \tag{7b}$$

where $\epsilon_i^m$ is an intermediate strain of the beam.

## III. Results and Discussion

We now discuss the results of our numerical simulations, obtained by solving (1)–(7) self consistently. The numerical algorithm is summarized in section III of the Appendix. We first explain, as a reference point, the response of pristine MEMS (without dielectric charging and creep) and discuss its static and dynamic behaviors in Sections III-A and B. We then discuss how the effect of dielectric charging and creep modifies the response of RF MEMS over time. While the results are obtained for the specific numerical solution of a switch/varactor with fixed-fixed beam, the generality of the arguments suggests that these results may be broadly applicable to wider range of MEMS configurations.

### *A. Static Behavior: CV Characteristics and Beam Shapes*

The steady-state shapes of the beam for various applied voltages are computed by time-independent solutions of (1) and (2), and are shown in Fig. 4(a) and (b). The stress voltage has been ramped up from 0 V to 60 V, and then ramped down to 0 V. In response, the beam bends toward the dielectric symmetrically

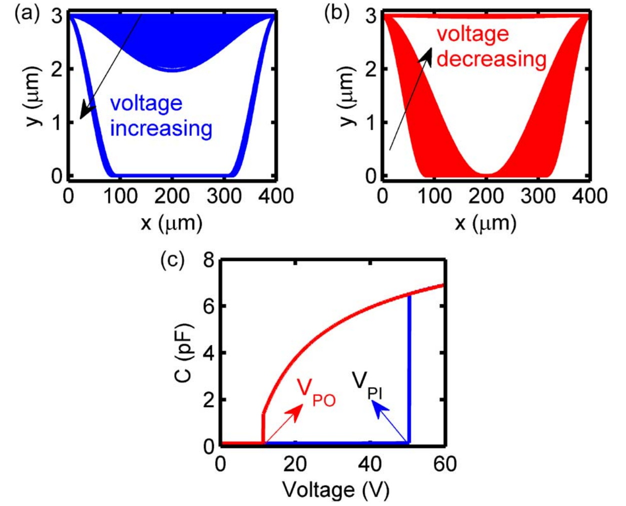


Fig. 4. (a) and (b) Steady-state shapes of the beam when the voltage is increasing (a) and when it is decreasing (b). (c) The CV curve of a RF MEMS capacitive switch. Abrupt jump in capacitance at $Vp_I$ (when voltage is increasing) is due to pull-in behavior of the device. A correspond jump in capacitance is also observed during pull-out $(Vp_O)$, when voltage is decreasing. Varactor operates in the up state, with $V < Vp_I$.

[Fig. 4(a)], with a corresponding increase in the capacitance (Fig. 4(c), bottom branch). When $V > Vp_I$, $F_{\text{electrostatic}}$ exceeds spring-like restoring force [fourth-order derivative term in (1)], and beam is abruptly pulled in to rest on the dielectric [Fig. 4(a)]. This pull-in behavior causes the capacitance $(C)$ to jump discontinuously from the lower to the upper branch [Fig. 4(c)]. Incidentally, this transition is analogous to a phase transition in thermodynamics, with displacement $y$ being the order parameter and $V$ being the forcing function [42]. Any further increase in $V$ increases the contact area [Fig. 4(a)], and hence, the capacitance of the device [Fig. 4(c)]. In the reverse cycle, when voltage is ramped down, the contact area reduces gradually [Fig. 4(b)], and so does the capacitance [Fig. 4(c)]. At $V = Vp_O$, the beam barely touches the dielectric at a single point, which is shown in Fig. 4(b). When $V < Vp_O$, beam is released from the dielectric and comes back in air [Fig. 4(b)].

### *B. Pull-in Dynamics: Effect of Voltage and Pressure*

For pull-in dynamics of the switch, we solve (1) and (2) in response to a step voltage. The corresponding shapes of the beam, displacement, and velocity of the center of the beam as a function of time are shown in Fig. 5(a) and (b), respectively. We define $tp_I$ as the pull-in time needed for the upper electrode to reach the dielectric from its up state position, and $v_{\text{impact}}$ as the impact velocity with which the upper electrode lands on the dielectric. The rapid increase in the velocity near the contact [Fig. 5(b)] reflects the rapid increase in $F_{\text{electrostatic}}$ close to the contact (when $y \approx 0$). Fig. 5(c) shows $tp_I$ and $v_{\text{impact}}$ as a function of the applied voltage $V$. As $V$ increases, $F_{\text{electrostatic}}$ increases as $\sim V^2$ (1) thereby decreasing $tp_I$ and increasing $v_{\text{impact}}$. Our numerical simulation shows that $v_{\text{impact}}$ increases almost linearly with voltage $(v_{\text{impact}} \propto V)$, and $tp_I$ decreases as $tp_I \propto (1/V)$ [Fig. 5(c)]. Another important factor in determining $tp_I$ and $v_{\text{impact}}$ is the squeeze film gas damping, which is dictated by the pressure $p$ of the ambient gas [31].

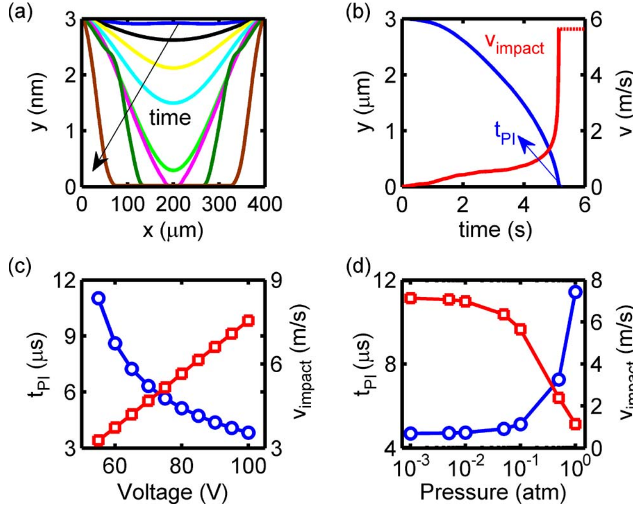


Fig. 5. Pull-in dynamics of the switch. (a) Shape of the fixed-fixed beam at different instants of the time during pull-in. Time is increasing in the direction of arrow. (b) Displacement (left axis) and velocity (right axis) of the center of beam during pull-in showing $tp_I$ and $v_{\mathrm{impact}}$. (c) Effect of voltage on pull-in dynamics of the switch. $tp_I$ (left axis, ○) decreases and $v_{\mathrm{impact}}$ (right axis,□) increases with voltage due to increase in the electrostatic force. (d) Effect of pressure on pull-in dynamics of the switch. When pressure is low, dynamics is inertia dominated and hence $tp_I$ (left axis, ○) and $v_{\mathrm{impact}}$ (right axis, □) are almost constant. Above a certain pressure (in our case ∼0.1 atm), pull-in dynamics becomes damping dominated, therefore, $tp_I$ and $v_{\mathrm{impact}}$ changes rapidly as a function of pressure.

As $p$ decreases, mean free path of gas molecules $(\lambda \propto 1/p)$ increases, and squeeze film gas damping is reduced [31]. This reduction in damping decreases $tp_I$ [Fig. 5(d)] and increases $v_{\mathrm{impact}}$ [Fig. 5(d)]. Fig. 5(d) also shows that $tp_I$ and $v_{\mathrm{impact}}$ are insensitive to pressure when $p$ is low (dynamics is dominated by inertia), whereas $tp_I$ increases and $v_{\mathrm{impact}}$ decreases rapidly above a critical pressure (in this case 0.1 atm), and dynamics become damping dominated. Apart from voltage and pressure, pull-in dynamics of the device is also affected by the charges inside the dielectric, and this will be discussed in the next section.

### *C. Reliability Implications of RF MEMS Capacitive Switch: Dielectric Charging*

Fig. 6 summarizes the predictions regarding the lifetime of the capacitive switch due to dielectric charging. Fig. 6(a) shows the evolution of electron number density $(n_T)$ inside the dielectric as a function of stress time when actuated by 80 V. The peak value of $n_T$ increases rapidly, and the centroid of $n_T$ profile moves away from the $M_1$-dielectric interface deeper into the dielectric as a function of contact duration. These negative charges within the dielectric increases the electrostatic force on the upper membrane (5), which makes the pull-in of the device easier (smaller $Vp_I$) and the pull-out difficult (smaller $Vp_O$). This reduction in $Vp_I/Vp_O$ shifts the CV curve to the left [Fig. 6(b)]. Fig. 6(c) shows $Vp_O$ as a function of stress time at different stress voltages. When $Vp_O$ crosses zero, electrode $M_1$ cannot be pulled-out even at zero applied voltage, because the electrostatic force by the negative charges becomes stronger than the restoring "spring" force of the beam. As a result, the device fails due to stiction. Using this time-dependent degradation of $Vp_O$, which is shown in Fig. 6(c), the dielectric limited

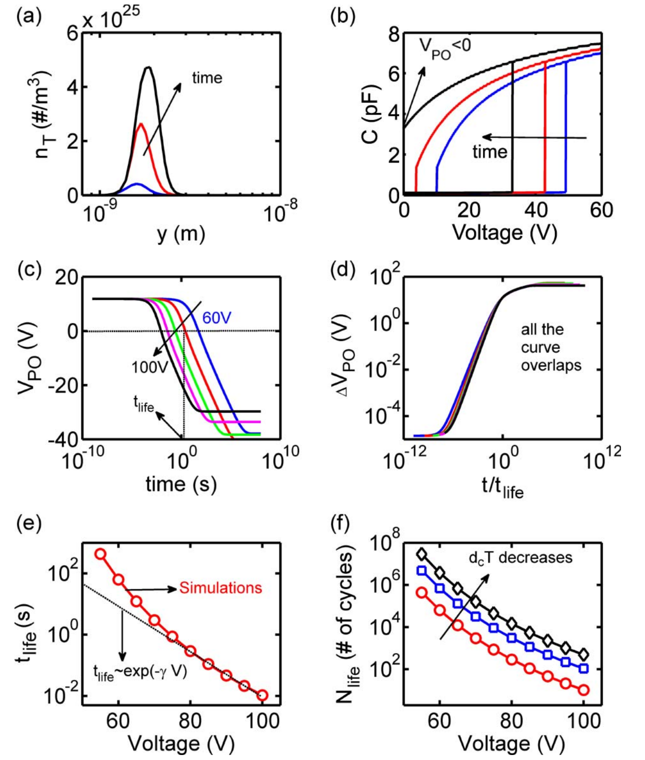


Fig. 6. Effect of dielectric charging on the performance and lifetime of a capacitive switch. (a) Electron number density $(n_T)$ inside the dielectric at different instants of the time, when stressed at 80 V. The peak value of $n_T$ increases, and centroid of $n_T$ profile moves deeper inside the dielectric with time. (b) The CV curve shifts to the left because of the accumulation of negative charges inside the dielectric (time increases in the direction of arrow). (c) $Vp_O$ plotted against stress time at various stress voltages. Stress voltage increases in the direction of arrow with an increment of 10 V. The device fails due to stiction when $Vp_O$ crosses zero. (d) When $\Delta Vp_O$ is plotted against $t/t_{\mathrm{life}}$, all the curves at different stress voltage overlap. (e) $t_{\mathrm{life}}$ of the device at different stress voltages. (f) The lifetime of the device defined by the number of cycles $(N_{\mathrm{life}})$ plotted as a function voltage, with $d_cT$ as a parameter, i.e., three characteristics for $d_cT = 1000\ \mu s$(○), $d_cT = 100\ \mu s$(□), $d_cT = 25\ \mu s$(◇), respectively.

lifetime $t_{\mathrm{life}}(V)$ can be obtained at arbitrary stress voltage by requiring that $Vp_O(t_{\mathrm{life}}) = 0$. This result is plotted in Fig. 6(e).

Interestingly, if we plot (without any *a priori* justification) $\Delta Vp_O$ against a new variable $t/t_{\mathrm{life}}(V)$, all the curves associated with different stress voltages overlap, i.e., $\Delta Vp_O \sim g(t/t_{\mathrm{life}})$, [Fig. 6(d)]. Although, we cannot offer an analytical derivation, our numerical simulation of fixed-fixed beam strongly suggests that

$$\Delta V_{pO} \sim g\left(\frac{t}{t_{\mathrm{life}}}\right) \approx 1 - \exp\left(-\left(\frac{t}{t_{\mathrm{life}}}\right)^{\beta}\right) \tag{8}$$

which reduces to a power law of the form, $\Delta Vp_O \sim (t/t_{\mathrm{life}})^{\beta}$, at short times. Here, $\beta$ is constant that depends on material parameters and device geometry. Based on some initial results, we speculate that $\Delta Vp_O = g(t/t_{\mathrm{life}})$ might apply to any MEMS geometry, where the functional form of $g$ can be obtained from experimental data for arbitrarily complex MEMS switches. If so, this scaling function offers a new algorithm for accelerated lifetime testing and would allow the device designer to determine $t_{\mathrm{life}}$ at reduced $V_{stress}$ based on the failure kinetics at higher applied biases.

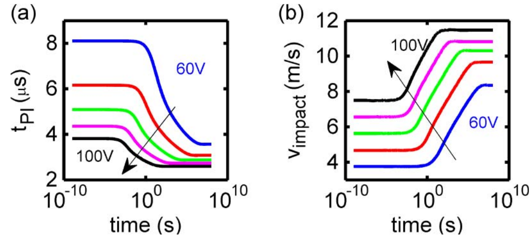


Fig. 7. Effect of dielectric charging on pull-in dynamics of the switch. (a) $tp_I$ decreases and (b) $v_{\text{impact}}$ increases with stress time due to accumulation of negative charges inside the dielectric. Actuation voltage increases in the direction of arrow with an increment of 10 V.

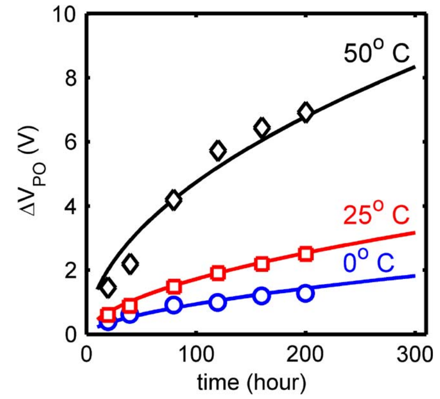


Fig. 8. Comparison of our theoretical model with the experimental data [43]. $\Delta Vp_O$ as a function of stress time for different temperatures. Symbols are the experimental data, and solid lines are predictions based on the model developed in this paper.

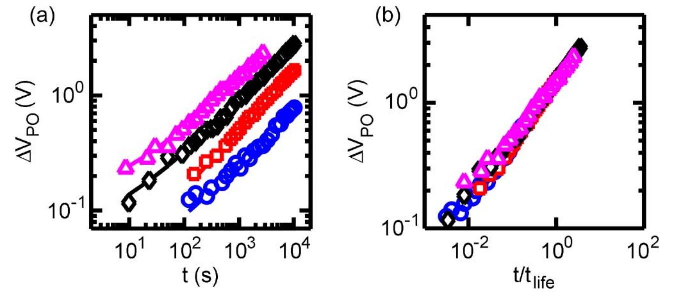


Fig. 9. Validation of scaling relationship against experimental data [44] (a) $\Delta Vp_O$ as a function of $t$ for four different stress voltages: 30 V (○), 35 V (□), 40 V (◇), 45 V (△). (b) When $\Delta Vp_O$ is plotted against $t/t_{\text{life}}$ assuming $Vp_O = 1.5$ V, all the curves overlap. This confirms the scaling behavior as anticipated in Fig. 6(d).

Regarding the second objective of the paper, in an operational circuit, the RF MEMS switch does not operate under dc bias, but is repeatedly turned on (pulled-in) and off (pulled-out). Therefore, we need to look into how repeated switching affects the lifetime. The dc $t_{\text{life}}$ can be viewed as a sum of the contact times during ac stress. Therefore, the number of cycles of safe operation $(N_{\text{life}})$ of the switch under ac stress can be deduced from dc $t_{\text{life}}$, as follows:

$$N_{\text{life}} = \frac{t_{\text{life}}}{d_c T - tp_I} \tag{9}$$

where $d_c$ is the duty cycle, and $f = 1/T$ is the frequency of the operation of actuation voltage. Equation (9) assumes that there is no relaxation of trapped charges during the time when voltage is removed. This simplifying assumption is justified by the fact that at the pulled-up state, the electric field across the dielectric is small (i.e., $E(y) \approx 0$), with correspondingly small emission current during off-state, i.e., $J_E(y) \approx 0$, from (12). Therefore, rate of relaxation of charges will be very small [$dn_T/dt \approx 0$, (4)]. It implies that during ac stress when voltage is removed, $\Delta Vp_O$ does not recover, but remains fixed at the same value, which it had at the end of previous stress cycle. Hence, an ac stress that toggles between 0 and $V$ does not improve integrated lifetime $(t_{\text{life}})$ of the switch, but it can only improve $N_{\text{life}}$ depending upon $d_c$ and $T$. Fig. 6(f) shows $N_{\text{life}}$ for different values of $d_cT$. $N_{\text{life}}$ increases as $d_cT$ decreases, because lower $d_cT$ implies shorter contact time per cycle. Moreover, since $d_cT - tp_I$ is the contact time for dielectric charging, $N_{\text{life}}$ increases significantly as $d_cT \to tp_I$.

We now focus on the third objective of the paper, related to the voltage acceleration model, i.e., the nonlinearity of $t_{\text{life}}(V)$ and $N_{\text{life}}(V)$ with $V$. Fig. 6(e) and (f) suggests that an empirical exponential model $t_{\text{life}}(V) \sim e^{-\gamma V}$, based on voltage acceleration coefficient $\gamma$ determined from the accelerated tests, might severely underestimate the lifetime of RF MEMS switches at operating voltages. Therefore, a more physics-based model like the one discussed in this paper is needed to correctly predict $t_{\text{life}}/N_{\text{life}}$ of the switch.

Dielectric charging not only affects the static behavior ($Vp_I$, $Vp_O$ and CV curve) of the device, but also affects the pull-in dynamics ($tp_I$ and $v_{\text{impact}}$) and the understanding of this phenomenon is the fourth objective of the paper. Fig. 7(a) and (b) shows $tp_I$ and $v_{\text{impact}}$ as a function of total integrated stress time at different actuation voltages. The trapped charges inside the dielectric increases the electrostatic force, and therefore, decreases $tp_I$ [Fig. 7(a)], and increases $v_{\text{impact}}$ [Fig. 7(b)]. The increase in $v_{\text{impact}}$ will degrade the dielectric surface through increased heat dissipation at the surface. The degraded surface may have higher adhesion force [8], thereby increasing the chances of failure due to stiction. We believe that the change in $tp_I$ or $v_{\text{impact}}$ as a function of stress time can also be used to monitor the charge injection inside the dielectric, but a quantitative model requires further work.

Finally, to validate the model just developed, we interpret the data from the literature through two nontrivial predictions of our model. Fig. 8 shows $\Delta Vp_O$ as a function of stress time for different temperatures [43]. Our simulation matches very well with the experimental data [43] and suggests that the model is physically justified. The temperature dependence in our model comes from temperature-activated FP emission current $J_E(y)$, see (12).

As a second validation, we explore the validity of the novel scaling relationship proposed in Fig. 6(d) by using the experimental data from [44]. Fig. 9(a) shows $\Delta Vp_O$ as a function of time for four different stress voltages. When this $\Delta Vp_O$ is plotted against $t/t_{\text{life}}$, assuming $Vp_O = 1.5$ V, all the curves overlap [Fig. 9(b)], which is consistent with (8) and anticipated by our numerical model.

To summarize this section, we have provided a theoretical framework for parametric degradation of $Vp_I, Vp_O, tp_I$ and $v_{\text{impact}}$ and $t_{\text{life}}/N_{\text{life}}$ prediction due to dynamic charge injection inside the dielectric. These results confirm that the physical

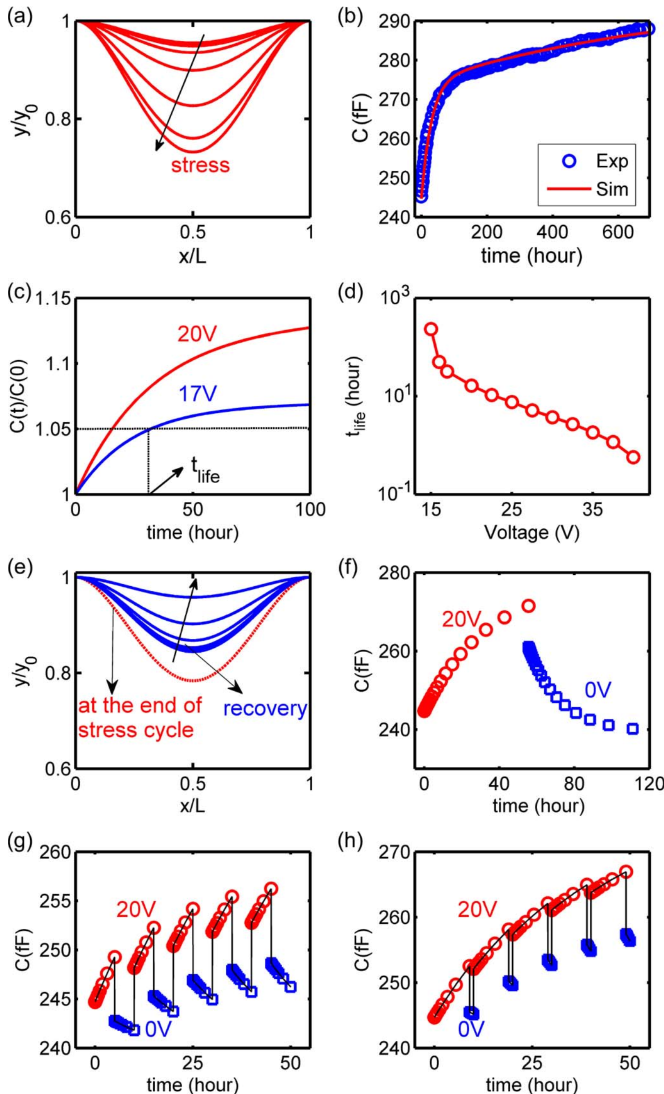


Fig. 10. Creep behavior of RF MEMS varactors (a) shape of the fixed-fixed beam during dc stress. Beam moves further down from its steady-state position due to creep causing (b) capacitance of the device to increase as a function of time. Our theoretical model predicts very well the experimentally observed capacitance change [23]. (c) Capacitance change as a function of time for two different applied voltages. (d) $t_{\mathrm{life}}$ as a function of applied voltage due to creep. $t_{\mathrm{life}}$ increases rapidly at low-stress voltages. (e) Shape of the fixed-fixed beam during stress recovery. When voltage is removed, beam does not go all the way up, it goes up to a certain amount, and then it recovers slowly which is reflected in (f) the capacitance of the device as a function of time. (g) and (h) Capacitance of the device as a function of time during ac stress. When a square voltage waveform of period 10 h is applied, then at high voltage, capacitance goes up due to creep, and when voltage is removed, capacitance slowly recovers. Recovery depends on the duty cycle of the waveform. At (g) duty cycle of 50%, recovery is more as compared to (h) duty cycle of 90%.

model may help interpret many features of the experimental data that could not be analyzed by simpler empirical models.

### *D. Reliability Implication for RF MEMS Varactor: Creep*

The last three objectives of the paper involve exploring creep-limited lifetime of RF MEMS varactor. Fig. 10 shows the results of time-dependent creep, obtained by solving (7). We first validate the theoretical model by comparing against experimental data [23] based on nickel (Ni) membrane. Fig. 10(b) shows the capacitance of the device at $V = 20$ V as a function of stress time. Using a three branch model of viscoelasticity, our model predictions reproduce the experimental features of creep degradation reasonably well [23]. The corresponding shapes of the beam at different instants of time are shown in Fig. 10(a). Ideally, with the application of a dc voltage ($V < Vp_I$), the fixed-fixed beam should move down [Fig. 10(a)] and come to steady state at a position defined by the balance of "spring" and electrostatic force. However, the beam continues to be pulled down [Fig. 10(a)] as a function of time due to creep, as predicted by (7).

The experimentally validated model offers us an opportunity to explore the creep behavior of varactor at different voltages. The time-dependent change in capacitance for two different operating voltages are shown in Fig. 10(c). This change in capacitance degrades circuit performance, that is, an oscillator circuit will no longer remain tuned at the desired frequency due to the creep-induced capacitance change, and an external feedback circuit that compensates for the capacitance change will be necessary for the correct operation of the circuit. To quantify the capacitance degradation, we define the creep-limited lifetime as being the time in which capacitance changes by a fixed percentage of the capacitance at $t = 0$, i.e., $(C(t_{\mathrm{life}}) - C(0))/C(0) = r$, where $C(t_{\mathrm{life}})$ is the capacitance at $t = t_{\mathrm{life}}$ and $C(0)$ is the capacitance at $t = 0$ at the operating voltage $V$, and $r$ is the tolerance limit for degradation. For example, Fig. 10(a) shows creep-limited lifetime for as a function of stress voltage for $r = 0.05$. As operating voltage increases, the lifetime reduces exponentially. The voltage acceleration observed here is mainly due to spring-softening effect, which effectively weakens the spring as a function of stress voltage.

When the voltage is removed, the beam should ideally be restored to the initial position of zero deflection, but creep prevents this instant restoration of the pristine beam shape [Fig. 10(e)]. Instead, the beam (and the capacitance) is restored asymptotically to the original shape over a long period of time [Fig. 10(f)]. In practice, however, device is operated continuously, and voltage is applied repeatedly. For such an ac stress, Fig. 10(g) and (h) show the capacitance of the device at stress voltage and at zero voltage. When the voltage is applied, the capacitance continues to increase due to creep, and when voltage is removed, it recovers slowly. If the time allowed for recovery is insufficient, residual capacitance at zero voltage increases with number of cycles [Fig. 10(g) and (h)]. This increase in the capacitance at zero voltage is higher for higher duty cycle [Fig. 10(g) and (h)], because less time is available for recovery. We want to mention here that the effect of cyclic loading and duty cycle on creep dynamics has also been studied in literature [22] though in the context of a capacitive switch.

To summarize this section on creep, our analysis shows that creep can be incorporated in the EB equation framework using viscoelastic theory. The framework presented can explain the experimentally observed time-dependent capacitance change and offers the possibility to predict creep-limited lifetime for arbitrary voltages. However, we want to mention here that our analysis does not account for residual stress which people have looked into to some extent in the context of a capacitive switch [45]. Even though their approach is similar to our approach, they use a simple analytical formula for the calculation of

restoring force, whereas we do full numerical simulation of EB equation.

## IV. Conclusion

In this paper, we have presented a physics-based theoretical modeling framework for the dominant degradation mechanisms of RF MEMS capacitive switches and varactors. Specifically, our model can predict, for arbitrary bias conditions, the drift of the parameters $(Vp_I, Vp_O, tp_I, v_{\text{impact}}, C)$ of a capacitive switch or a varactor over time. Based on this models of parametric degradation, one can reliably predict the RF MEMS lifetime defined by the dielectric charging and/or creep. For dielectric charging, the model offers scaling relationship for $\Delta Vp_O$, more optimistic voltage acceleration models $(t_{\text{life}} > \exp(-\gamma V))$, and explains how lifetime improves at higher frequency and reduced duty cycle. Likewise, the experimentally validated creep model suggests opportunities of improving creep performance at reduced voltage [Fig. 10(d)] and higher operating frequency and reduced duty cycle.

Even though our modeling framework integrates and generalizes several existing models in the literature and offers many new insights regarding reliability of RF MEMS, there are scopes for further refinement by including fringing fields for the electrostatic force, residual stress in the fixed-fixed beam, midplane stretching [34], and surface roughness of the dielectric for dielectric charging [46], [47]. Similarly, although the model is validated against a number of experimental results from the literature, a broader experimental validation of the effects of dielectric charging on pull-in dynamics, creep-limited lifetime, effect of duty cycle on creep induced degradation, etc., could be pursued in future experiments.

Our modeling framework is an important step toward reliability aware design/optimization of a capacitive switch or varactors. Moreover, our physics-based modeling framework both for dielectric charging and creep will offer more than just reliable lifetime prediction and help designers/experimentalist improve the device design/process flow by correctly identifying the critical parameters responsible for such degradations.

## Appendix

### I. Dielectric Charging

The electron injection current from the metal contacts into a trap located at a distance $y$ from the contact—$J_{IN}(y)$ is given by a modified form of the Tsu-Esaki equation [48]:

$$J_{IN}(y) = \frac{4\pi m^- q}{h^3}\sigma\Delta y\,[N_T(y) - n_T(y)] \times \int_{-\infty}^{\infty} T^r(E,y)\beta_1(E,y)S(E)f(E)dE \tag{10a}$$

$$J_{IN}(y) = A_{IN}(y)\,[N_T(y) - n_T(y)] \tag{10b}$$

where the factor $\sigma\Delta y[N_T(y) - n_T(y)]$ is the integrated capture cross sections of all the empty traps inside a region of width $\Delta y$. $T^r(E,y)$ is the elastic *transmission tunneling probability* of electrons from the metal contacts to a distance $y$ into the dielectric at an energy $E$ and can be calculated by the Wentzel-Kramers-Brillouin approximation [49]. $S(E)$ is called the *supply function* and is obtained by integrating the lateral momentum of the electrons inside the metal over the energy. The *Fermi-Dirac distribution* function $f(E)$ gives the fraction of occupied states, and therefore the fraction of electrons available for injection at energy $E$ from the contact metal work function $(E_F)$. We account for the phonon scattering for the electron tunneling from the contacts to relax into the trap energy level, through a *scattering factor*$\beta_1(E,y)$.

Similarly, the flux of trapped electrons leaking back to the empty states in the metal by tunneling can be expressed as follows:

$$J_{OUT}(y) = \frac{4\pi m^- q}{h^3}\sigma\Delta y\,[n_T(y)] \times \int_{-\infty}^{\infty} T^r(E,y)\beta_2(E,y)S(E)(1-f(E))dE \tag{11a}$$

$$J_{OUT}(y) = A_{OUT}(y)n_T(y). \tag{11b}$$

Here, the term $\sigma\Delta y[n_T(y)]$ represents the ratio of the effective area of all filled traps inside a region of width $\Delta y$ within the insulator, to the total cross section of the metal-insulator contact interface, and the term $1 - f(E)$ denotes the fraction of empty states in the metal as a function of energy $E$.

The trapped electrons can also escape from the traps into the dielectric conduction band by a temperature-activated, field-assisted FP emission process [50], [51]. Higher electric field reduces the effective trap depth of a negatively charged (filled) trap. The expression for the FP emission flux $(J_E(y))$ is given by

$$J_E(y) = \gamma q\Delta y\,[n_T(y)]\exp\left(-\frac{\Phi_T - \sqrt{\frac{q^3 E(y)}{\pi\epsilon_0\epsilon_\infty}}}{k_B T}\right) \tag{12a}$$

$$J_E(y) = A_E(y)n_T(y). \tag{12b}$$

Here, $\gamma$ is the attempt frequency [52] and $\epsilon_\infty$ is the high frequency dielectric constant of the insulator, and equals the square of its refractive index [53].

### II. Creep

Using the spring-dashpot model of Fig. 3 and (6), we can obtain the following equations:

$$\frac{-Mu}{IE_i} = \frac{\eta_i}{E_i}\frac{d\left(-u\frac{\partial^2 y_i}{\partial x^2}\right)}{dt} - u\frac{\partial^2 y_i}{\partial x^2}, \quad i = 2, 3, \ldots n \tag{13}$$

$$-u\frac{\partial^2 y}{\partial x^2} = \frac{-Mu}{IE_1} - \sum_{2}^{n} u\frac{\partial^2 y_i}{\partial x^2} \tag{14}$$

where $\sigma = -(Mu/I)$, $\epsilon = -u(\partial^2 y_i/\partial x^2)$, and $u$ is the distance of a point on the beam from its neutral axis, which is at the center of the beam for a rectangular cross-sectional beam. On differentiating (13) and (14) twice with respect to $x$, and using $F_{\text{electrostatic}} = \partial^2 M/\partial x^2$ and $\epsilon_i^m = \partial^4 y_i/\partial x^4$, we get (7a) and (7b).

### III. Numerical Methods

*1) Static Behavior (Beam Shape and CV Curve):* The static behavior of a fixed-fixed beam with voltage $V$ is governed by (1), with time derivative set to zero. To solve (1) numerically, it is discretized using a simple finite difference technique with constant grid size of $\Delta x = L/(N-1)$, where $N$ is the total number of nodes used for discretization. We also change the variable from $y$ to $y_0 - y$. The boundary conditions of (2) can be written in terms of the displacement of nodes 1, 2, $N, N-1$ as follows:

$$y_1 = y_N = 0 \tag{15a}$$
$$y_2 = y_{N-1} = 0. \tag{15b}$$

At any generic node $i$, the discretized form of (1) is given by:

$$y_{1+2} - 4y_{i+1} + 6y_i - 4y_{i-1} + y_{i-2} = \frac{(\Delta x)4}{D} F_{\text{electrostatic}}(xi, yi) \tag{16}$$

where $y_i$ is the displacement of the node $i$, $D = EI/(1-v^2)$, and $F_{\text{electrostatic}}$ is the electrostatic force acting on the node $i$, where $i = 3, 4, \ldots, N-3, N-2$. Equations (15) and (16) can be rewritten in the form of a matrix as follows:

$$[A][Y] = [F] \tag{17}$$

where $[A]$ is the coefficient matrix, $[Y]$ is the displacement vector, and $[F]$ is the force vector. Equation (17) is a nonlinear equation, because $F_{\text{electrostatic}}(x_i, y_i)$ depends on $y_i$; therefore, it is solved iteratively to obtain the shape of the beam for a given voltage $V$.

*2) Dynamic Behavior (Pull-in Time and Impact Velocity):* The dynamics of the fixed-fixed beam in response to an applied voltage $V$ is again described by (1). Once again, with the change of the variable from $y$ to $y_0 - y$, initial conditions of the beam dynamics are given as follows:

$$y(x,0) = 0 \tag{18a}$$
$$v(x,0) = \frac{\partial y}{\partial t}(x,0) = 0 \tag{18b}$$

where $v(x,t)$ is the velocity of a point at location $x$ on the beam and at time $t$. (18b) signifies that beam starts from rest. Using the forward difference technique, for any generic node $i$, (1) can be written as follows:

$$\rho_l \frac{v_i(t+\Delta t) - v_i(t)}{\Delta t} + b\left(y_i(t)\right) v_i(t) + \frac{EI}{1-v^2}\frac{\partial^4 y_i}{\partial x^4} = F_{\text{electrostatic}}(x_i, y_i) \tag{19}$$

where $\Delta t$ is the time step. Equation (19) can be rewritten to obtain the velocity of node $i$ at time $t + \Delta t$ as follows:

$$v_i(t+\Delta t) = v_i(t) + \frac{\Delta t}{\rho l}\left(F_{\text{electrostatic}}(x_i, y_i) - b\left(y_i(t)\right) v_i(t) - \frac{EI}{1-v^2}\frac{y_{i+2} - 4y_{i+1} + 6y_i - 4y_{i-1} + y_{i-2}}{(\Delta x)4}\right). \tag{20}$$

Now, the displacement of any node $i$ can be computed from its velocity as follows:

$$y_i(t+\Delta t) = y_i(t) + \Delta t v_i(t+\Delta t). \tag{21}$$

*3) Dielectric Charging:* Equations (4) and (5) can be written for all the grid points between $y = -y_d$ and $y = 0$ and then converted in the form of a matrix equation as follows:

$$\frac{dN(t)}{dt} = A_N N(t) + D \tag{22}$$

where

$$A_N = -\begin{bmatrix} A_{IN}(y=0) + A_{OUT}(y=0) + A_E(y=0) \\ A_{IN}(y=\Delta y) + A_{OUT}(y=\Delta y) + A_E(y=\Delta y) \\ \vdots \\ A_{IN}(y=-y_{\text{d}}) + A_{OUT}(y=-y_{\text{d}}) + A_E(y=-y_{\text{d}}) \end{bmatrix} \tag{23a}$$

$$D = \begin{bmatrix} A_{IN}(y=0) N_T(y=0) \\ A_{IN}(y=\Delta y) N_T(y=\Delta y) \\ \vdots \\ A_{IN}(y=-y_d) N_T(y=-y_d) \end{bmatrix} \tag{23b}$$

$$N(t) = \begin{bmatrix} n_T(y=0,t) \\ n_T(y=\Delta y,t) \\ \vdots \\ n_T(y=-y_d,t) \end{bmatrix}. \tag{23c}$$

Equation (22) can be discretized in time to calculate time dynamics of $n_T(y,t)$ using the more stable Backward Euler method as follows:

$$\frac{N(t+\Delta t) - N(t)}{\Delta t} = A_N N(t+\Delta t) + D. \tag{24}$$

Equation (24) can be rearranged to obtain a linear system for $(t + \Delta t)$ as follows:

$$[I - A_N \Delta t] N(t+\Delta t) = [N(t) + D\Delta t]. \tag{25}$$

Now, (25) is solved using the CSparse library.

*4) Creep:* The effect of creep on the behavior of varactor is studied using (7). To solve (7), we start with the following initial conditions for intermediate strain (strain is zero at $t = 0$):

$$\epsilon_i^m(x,0) = 0, \quad i = 2, 3 \ldots, n. \tag{26}$$

The time evolution of strain and $F_{\text{electrostatic}}$ can be computed, as follows:

$$\epsilon_i^m(x, t+\Delta t) = \epsilon_i^m(t) + \frac{\Delta t E_i}{\eta_i}\left(\frac{F_{\text{electrostatic}}}{E_1 I} - \epsilon_i^m(x,t)\right). \tag{27}$$

Once the strain is obtained, the shape of the beam is obtained by solving (28) which is

$$E_1 I \frac{\partial^4 y}{\partial x^4} = F_{\text{electrostatic}} + E_1 I \sum_2^n \epsilon_i^m. \tag{28}$$

Equations (27) and (28) are coupled through $F_{\text{electrostatic}}$ and $\epsilon_i^m$, and hence are solved iteratively self-consistently at each time $t$.

## ACKNOWLEDGMENT

The authors gratefully acknowledge discussions with Prof. A. Alexeenko, Prof. J. Murthy, Prof. D. Peroulis, Prof. A. Raman, and Prof. M. Koslowski. They also are grateful for the computational resources from the Network for Computational Nanotechnology (NCN).

## REFERENCES

[1] H. De Los Santos, G. Fischer, H. Tilmans, and J. van Beek, "RF MEMS for ubiquitous wireless connectivity: Part 2—Application," *IEEE Microw. Mag.*, vol. 5, no. 4, pp. 50–65, Dec. 2004.

[2] J. Yao, "RF MEMS from a device perspective," *J. Micromech. Microeng.*, vol. 10, no. 4, pp. R9–R38, Dec. 2000.

[3] G. M. Rebeiz and J. B. Muldavin, "RF MEMS switches and switch circuits," *IEEE Microw. Mag.*, vol. 2, no. 4, pp. 59–71, Dec. 2001.

[4] I. De Wolf and W. van Spengen, "Techniques to study the reliability of metal RF MEMS capacitive switches," *Microelectron. Reliab.*, vol. 42, no. 9–11, pp. 1789–1794, Sep.–Nov. 2002.

[5] K. Komvopoulos, "Surface engineering and microtribology for microelectromechanical systems," *Wear*, vol. 200, no. 1/2, pp. 305–327, Dec. 1996.

[6] W. van Spengen, "MEMS reliability from a failure mechanisms perspective," *Microelectron. Reliab.*, vol. 43, no. 7, pp. 1049–1060, Jul. 2003.

[7] G. Gregori and D. Clarke, "Mechanical creep as a life-limiting factor of radio frequency microswitches," *Appl. Phys. Lett.*, vol. 87, no. 15, pp. 154 101-1–154 101-3, Oct. 2005.

[8] M. Philippine, S. Timpe, and K. Komvopoulos, "Evolution of interfacial adhesion force in dynamic micromachines due to repetitive impact loading," *Appl. Phys. Lett.*, vol. 91, no. 6, pp. 063102-1–063102-3, Aug. 2007.

[9] S. Patton and J. Zabinski, "Effects of dielectric charging on fundamental forces and reliability in capacitive microelectromechanical systems radio frequency switch contacts," *J. Appl. Phys.*, vol. 99, no. 9, p. 094910-1–094910-11, May 2006.

[10] C. Goldsmith, J. Ehmke, A. Malczewski, B. Pillans, S. Eshelman, Z. Yao, J. Brank, and M. Eberly, "Lifetime characterization of capacitive RF MEMS switches," in *IEEE Microw. Symp. Tech. Dig.*, 2001, pp. 227–230.

[11] X. Yuan, S. Cherepko, J. Hwang, C. L. Goldsmith, C. Nordqusit, and C. Dyck, "Initial observation and analysis of dielectric-charging effects on RF MEMS capacitive switches," in *IEEE Microw. Symp. Tech. Dig.*, 2004, pp. 1943–1946.

[12] X. Yuan, J. C. M. Hwang, D. Forehand, and C. L. Goldsmith, "Modeling and characterization of dielectric-charging effects in RF MEMS capacitive switches," in *IEEE Microw. Symp. Tech. Dig.*, 2005, pp. 753–756.

[13] W. van Spengen, R. Puers, R. Mertens, and I. De Wolf, "A comprehensive model to predict the charging and reliability of capacitive RF MEMS switches," *J. Micromech. Microeng.*, vol. 14, no. 4, pp. 514–521, Apr. 2004.

[14] X. Yuan, Z. Peng, J. Hwang, D. Forehand, and C. Goldsmith, "Acceleration of dielectric charging in RF MEMS capacitive switches," *IEEE Trans. Device Mater. Rel.*, vol. 6, no. 4, pp. 556–563, Dec. 2006.

[15] X. Rottenberg, B. Nauwelaers, W. De Raedt, and H. A. C. Tilmans, "Distributed Dielectric charging and its impact on RF MEMS devices," in *Proc. Eur. Microw. Conf.*, 2004, pp. 77–80.

[16] X. Rottenberg, I. De Wolf, B. Nauwelaers, W. De Raedt, and H. Tilmans, "Analytical model of the DC actuation of electrostatic MEMS devices with distributed dielectric charging and nonplanar electrodes," *J. Microelectromech. Syst.*, vol. 16, no. 5, pp. 1243–1253, Oct. 2007.

[17] C. L. Goldsmith, D. I. Forehand, Z. Peng, J. C. M. Hwang, and I. L. Ebel, "High-cycle life testing of RF MEMS switches," in *IEEE Microw. Symp. Tech. Dig.*, 2007, pp. 1805–1808.

[18] S. Melle, D. De Conto, D. Dubuc, K. Grenier, O. Vendier, J. Muraro, J. Cazaux, and R. Plana, "Reliability modeling of capacitive RF MEMS," *IEEE Trans. Microw. Theory Tech.*, vol. 53, no. 11, pp. 3482–3488, Nov. 2005.

[19] P. Mark and T. Hartman, "On distinguishing between the Schottky and Poole-Frenkel effects in insulators," *J. Appl. Phys.*, vol. 39, no. 4, pp. 2163–2164, Mar. 1968.

[20] H. H. Hsu and D. Peroulis, "A viscoelastic-aware experimentally derived model for analog RF-MEMS varactors," in *Proc. IEEE MEMS*, 2010, pp. 783–786.

[21] M. V. Gils, J. Bielen, and G. McDonald, "Evaluation of creep in RF MEMS devices," in *Proc. EuroSime*, 2007, pp. 1–6.

[22] X. Yan, W. Brown, Y. Li, J. Papapolymerou, C. Palego, J. Hwang, and R. Vinci, "Anelastic stress relaxation in gold films and its impact on restoring forces in MEMS devices," *J. Microelectromech. Syst.*, vol. 18, no. 3, pp. 570–576, Jun. 2009.

[23] H.-H. Hsu and D. Peroulis, "A CAD model for creep behavior of RF-MEMS varactors and circuits," *IEEE Trans. Microw. Theory Tech.*, vol. 59, no. 7, pp. 1761–1768, Jul. 2011.

[24] A. F. Marques, R. C. Castello, and A. M. Shkel, "Modelling the electrostatic actuation of MEMS: State of the art," Universitat Politècnica de Catalunya, Barcelona, Spain, Tech. Rep. IOC-DT-P-2005-18, 2005.

[25] V. Leus and D. Elata, "On the dynamic response of electrostatic MEMS switches," *J. Microelectromech. Syst.*, vol. 17, no. 1, pp. 236–243, Feb. 2008.

[26] M. Younis, E. Abdel-Rahman, and A. Nayfeh, "A reduced-order model for electrically actuated microbeam-based MEMS," *J. Microelectromech. Syst.*, vol. 12, no. 5, pp. 672–680, Oct. 2003.

[27] A. H. Nayfeh and M. I. Younis, "A new approach to the modeling and simulation of flexible microstructures under the effect of squeeze film damping," *J. Micromech. Microeng.*, vol. 14, no. 2, pp. 170–181, Feb. 2004.

[28] R. C. Batra, M. Profiri, and D. Spinello, "Electromechanical model of electrically actuated narrow microbeams," *J. Microelectromech. Syst.*, vol. 15, no. 5, pp. 1175–1189, Oct. 2006.

[29] Y. Zhu and H. Espinosa, "Effect of temperature on capacitive RF MEMS switch performance—A coupled-field analysis," *J. Micromech. Microeng.*, vol. 14, no. 8, pp. 1270–1279, Aug. 2004.

[30] L. Zhang and Y. Zhao, "Electromechanical model of RF MEMS switches," *Microsyst. Technol.*, vol. 9, no. 6/7, pp. 420–426, Sep. 2003.

[31] X. Guo and A. Alexeenko, "Compact model of squeeze-film damping based on rarefied flow simulations," *J. Micromech. Microeng.*, vol. 19, no. 4, p. 045 026, Apr. 2009.

[32] M. Bao and H. Yang, "Squeeze film air damping in MEMS," *Sens. Actuators A, Phys.*, vol. 136, no. 1, pp. 3–27, May 2007.

[33] H. Sumali, "Squeeze-film damping in the free molecular regime: Model validation and measurement on a MEMS," *J. Micromech. Microeng.*, vol. 17, no. 11, pp. 2231–2240, Nov. 2007.

[34] E. Abdel-Rahman, M. Younis, and A. Nayfeh, "Characterization of the mechanical behavior of an electrically actuated microbeam," *J. Micromech. Microeng.*, vol. 12, no. 6, pp. 759–766, Nov. 2002.

[35] A. Chowdry and C. R. Westgate, "The role of bulk traps in metal-insulator contact charging," *J. Phys. D, Appl. Phys.*, vol. 7, no. 5, pp. 713–725, Mar. 1974.

[36] D. A. Buchanan, R. A. Abram, and M. J. Morant, "Charge trapping in silicon-rich $Si_3N_4$ thin films," *Solid State Electron.*, vol. 30, no. 12, pp. 1295–1301, Dec. 1987.

[37] R. Ramprasad, "Phenomenological theory to model leakage currents in metal–insulator–metal capacitor systems," *Phys. Stat. Sol. (B)*, vol. 239, no. 1, pp. 59–70, Sep. 2003.

[38] M. Exarchos, V. Theonas, P. Pons, G. Papaioannou, S. Melle, D. Dubuc, F. Cocetti, and R. Plana, "Investigation of charging mechanisms in metal-insulator-metal structures," *Microelectron. Reliab.*, vol. 45, no. 9–11, pp. 1782–1785, Sep.–Nov. 2005.

[39] P. C. Arnett and B. H. Yun, "Silicon nitride trap properties as revealed by charge-centroid measurements on MNOS devices," *Appl. Phys. Lett.*, vol. 26, no. 3, pp. 94–96, Feb. 1975.

[40] J. Li and A. Dasgupta, "Failure-mechanism models for creep and creep rupture," *IEEE Trans. Rel.*, vol. 42, no. 3, pp. 339–353, Sep. 1993.

[41] D. Roylance, *Engineering Viscoelasticity*. Cambridge, MA: MIT Press, 2001.

[42] A. B. Pippard, *Response and Stability*. Cambridge, U.K.: Cambridge Univ. Press, 1985.

[43] X. Yuan, Z. Peng, J. C. M. Hwang, D. Forehand, and C. L. Goldsmith, "Temperature acceleration of dielectric charging in RF MEMS capacitive switches," in *Proc. IEEE Microw. Symp. Dig.*, 2006, pp. 47–50.

[44] R. W. Herfst, P. G. Steeneken, and J. Schmitz, "Time and voltage dependence of dielectric charging in RF MEMS capacitive switches," in *Proc. IEEE Int. Rel. Phys. Symp.*, 2007, pp. 417–421.

[45] M. McLean, W. Brown, and R. Vinci, "Temperature-dependent viscoelasticity in thin Au films and consequences for MEMS devices," *J. Microelectromech. Syst.*, vol. 19, no. 6, pp. 1299–1308, Dec. 2010.

[46] P. Sumant, A. Cangellaris, and N. Aluru, "Modeling of dielectric charging in RF MEMS capacitive switches," *Microw. Opt. Technol. Lett.*, vol. 49, no. 12, pp. 3188–3192, Dec. 2007.

[47] P. Sumant, N. Aluru, and A. Cangellaris, "A compact model for dielectric charging in RF MEMS capacitive switches," *Int. J. RF Microw. Comput.-Aided Eng.*, vol. 19, no. 2, pp. 197–203, Mar. 2009.

[48] A. Gehring and S. Selberherr, "Modeling of tunneling current and gate dielectric reliability for nonvolatile memory devices," *IEEE Trans. Device Mater. Rel.*, vol. 4, no. 3, pp. 306–319, Sep. 2004.

[49] S. C. Miller, Jr. and R. H. Good, Jr., "A WKB-type approximation to the Schrodinger equation," *Phys. Rev.*, vol. 91, no. 1, pp. 174–179, Jul. 1953.

[50] R. B. Hall, "Poole-Frenkel effect," *Thin Solid Films*, vol. 8, no. 4, pp. 263–271, Oct. 1971.

[51] K. A. Nasyrov, V. A. Gritsenko, M. K. Kim, H. S. Chae, S. D. Chae, W. I. Ryu, J. H. Sok, J.-W. Lee, and B. M. Kim, "Charge transport mechanism in metal-nitride-oxide-silicon structures," *IEEE Electron Device Lett.*, vol. 23, no. 6, pp. 336–338, Jun. 2002.

[52] K. Lehovec and A. Fedotowsky, "Charge retention of MNOS devices limited by Frenkel-Poole detrapping," *Appl. Phys. Lett.*, vol. 32, no. 5, pp. 335–338, Mar. 1978.

[53] D. Jeong, H. Park, and C. Hwang, "Reasons for obtaining an optical dielectric constant from the Poole-Frenkel conduction behavior of atomic-layer-deposited $HfO_2$ films," *Appl. Phys. Lett.*, vol. 86, no. 7, pp. 072903-1–072903-3, Feb. 2005.

**Ankit Jain** received the B.Tech. degree in electrical engineering from the Indian Institute of Technology Kanpur, Kanpur, India, in May 2008. He is currently working toward the Ph.D. degree in the Department of Electrical and Computer Engineering, Purdue University, West Lafayette, IN, under the guidance of Prof. M. A. Alam.

His research interest mainly focuses on simulation, modeling, and reliability of nanoscale devices. Currently, he is working on reliability, nanostructured electrode design, and sensor applications of electromechanical devices like RF MEMS capacitive switches and nanoelectromechanical field effect transistor (NEMFET).

**Sambit Palit** (S'09) received the B.Tech. degree in electrical engineering and the M.Tech. degree in microelectronics from the Indian Institute of Technology Bombay, Mumbai, India in 2008. He is currently working toward the Ph.D. degree at Purdue University, West Lafayette, IN.

His current research interests include reliability modeling and electrical characterization of thin-film dielectric-based devices, and, more broadly, in modeling and simulation of micro- and nanoelectronic devices.

**Muhammad Ashraful Alam** (M'96–SM'01–F'06) received the Master's degree from Clarkson University, Potsdam, NY, in 1991, and the Doctoral degree from Purdue University, West Lafayette, IN, in 1995.

From 1995 to 2001, he was with Bell Laboratories, Murray Hill, NJ, as a Member of Technical Staff in the Silicon ULSI Research Department. From 2001 to 2003, he was a Distinguished Member of Technical Staff at Agere Systems, Murray Hill, NJ. During his time in industry, he made important contributions to reliability physics of electronic devices, metal-organic chemical vapor deposition crystal growth for optoelectronic integrated circuits, and performance limits of directly modulated semiconductor lasers. He is a Professor of electrical and computer engineering and a University Faculty Scholar at Purdue University, where his research and teaching focus on physics, simulation, characterization, and technology of classical and emerging electronic devices. After joining Purdue University in 2004, his research broadened to include nanocomposite flexible electronics, organic solar cells, and performance limits of nanobiosensors. He has published over 100 papers in international journals and has presented many invited and contributed talks at international conferences.

Prof. Alam is a Fellow of the American Physical Society. He also received the 2006 IEEE Kiyo Tomiyasu Award for contributions to device technology for communication systems.